Development of a Gaussian Approximation Potential for GaN with Point Defects and Mg Impurities

Yuki Ohuchi[1,3*], Robert Stella[2,3], and Lado Filipovic[2,3]
[1]Advanced Technology Laboratory, Fuji Electric Co., Ltd., Tokyo 191-8502, Japan
[2]CDL for Multi-Scale Process Modeling of Semiconductor Devices and Sensors at the
[3]Institute for Microelectronics, TU Wien, 1040 Vienna, Austria
Email: ohuchi@iue.tuwien.ac.at

***Abstract*—We present a new Gaussian approximation potential (GAP) for the Ga-N-Mg system, developed to accurately describe GaN containing point defects and Mg impurities. By carefully sampling a diverse set of defect-containing and doped structures, the potential reproduces the formation energies and diffusion barriers of point defects in GaN as calculated by density functional theory. Specifically, the GAP reproduces formation energies within a maximum deviation of 1.9 eV and diffusion barrier energies within 0.4 eV. This potential enables large-scale molecular dynamics simulations of defect dynamics in GaN, including the effects of Mg doping.**

***Keywords*—GaN, Mg doping, point defect, formation energy, diffusion barrier energy, Gaussian approximation potential (GAP)**

I. Introduction

Ion implantation is a key technique for doping semiconductors in power switching devices due to its cost-effectiveness and reliability. However, *p*-type doping of wurtzite GaN−one of the most promising wide band-gap semiconductors [1]−by Mg ion implantation remains challenging because of the resulting low carrier concentration. This issue is mainly attributed to the formation of residual defects, such as vacancy complexes and Mg segregation, induced during the implantation and the subsequent annealing [2]. The distribution of the defects results from interactions among them at the atomic scale, and depends on the processing conditions [3-5]. Understanding the dynamic behavior of these defects under different processing conditions is therefore crucial. Despite extensive experimental investigations to reveal the atomic-scale configurations and dynamics of the implantation-induced defects [6,7], the underlying mechanisms are still under discussion.

Molecular dynamics (MD) simulation is a highly effective method of analyzing defect behavior at the atomic scale. Although MD simulations based on density functional theory (DFT) provide the most reliable trajectories of atoms, the high computing cost makes it impractical to analyze large-scale models that include multiple defects in hundreds of atoms. Classical MD simulations have much lower computing costs. However, accurate and robust atomic interactions were difficult to define, resulting in limited insight into defect behavior [8,9]. Recent advances in machine-learned (ML) interatomic potentials have enabled large-scale simulation with accuracy comparable to that of DFT [10]. An interatomic potential applicable to MD simulations has also been reported for a Ga-N system using a neural network [11]. Nevertheless, developing an accurate potential that is transferable to systems containing both GaN and impurities like Mg is not trivial, because the configurational space grows significantly with the number of elements involved.

In this study, we develop an ML interatomic potential (IAP) to model defect behavior in GaN with Mg, enabling efficient and accurate simulation of defect dynamics in doped GaN systems.

II. Methods

The Gaussian approximation potential (GAP) [12,13] was employed as the IAP. GAP was selected for its favorable balance between accuracy and computational cost. Compared to the moment tensor potential (MTP), GAP provides higher fidelity in capturing complex atomic interactions, while neural network potentials may offer similar or even higher accuracy at a higher computational cost. We incorporated two-body and three-body interactions and the smooth overlap of atomic positions (SOAP) descriptor [14] to predict energy, as expressed in the following equation:

$$E = \sum_{d} \sum_{i} \sum_{j} \alpha_j^{(d)} K^{(d)} \left(x_i^{(d)}, x_j^{(d)} \right) \quad (1)$$

where *d* indexes the descriptor type (i.e. 2-body, 3-body, and SOAP descriptors), $x_i^{(d)}$ are descriptor vectors for input environment *i*, $\alpha_j^{(d)}$ are regression weights at the sparse training point *j*, and $K^{(d)}$is the kernel function for descriptor *d*.

Training data were derived from DFT calculations of cohesive energies and atomic forces, performed using Quantum ESPRESSO [15] with ultrasoft pseudopotentials and generalized gradient approximation for the exchange-correlation functional. Gallium 3*d* electrons were explicitly included in the

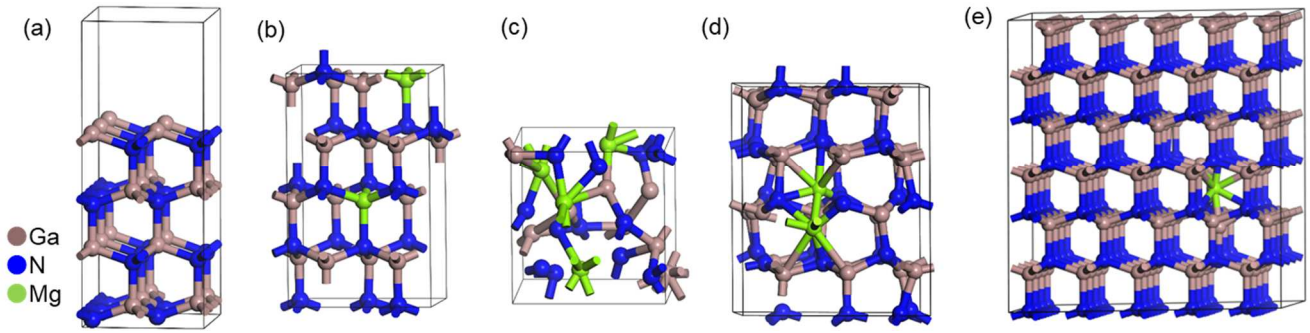

Fig. 1 Typical training structures: (a) GaN surface, (b) GaN with Mg defects, (c) distorted structures annealed at 5000 K, and snapshots of (d) molecular dynamics simulation and (e) barrier energy calculation by GAP.

valence shell. The cutoff energy was set to 680 eV and the *k*-space mesh was set below 0.08 $Å^{-1}$. All energy calculations were conducted under a neutral charge state.

We sampled atomic configurations from wurtzite GaN structures containing vacuum slabs and/or point defects, as shown in Figs. 1(a,b). To improve the GAP model's robustness, we also included virtual metastable crystals and distorted structures generated by first-principles MD simulations with various stoichiometries [Fig. 1(c)]. In addition, snapshots from MD simulations [Fig. 1(d)] and structures along diffusion pathways for barrier energy calculations by the nudged elastic band (NEB) method [Fig.1(e)]. These calculations were performed with our trained GAP model using the quip pair style implemented in the large-scale atomic/molecular massively parallel simulator (LAMMPS) [16]. The final dataset consisted of 4,950 structures, randomly divided into training and test data in an 8:2 ratio.

III. Results and Discussion

A. Training of GAP

Figs. 2(a,b) show comparisons of cohesive energies and atomic forces predicted by the trained GAP model against reference DFT values. The root mean square errors (RMSE) for both energy and force of the test data (8.1 meV/atom and 0.41 eV/Å) are comparable to those of the training dataset, indicating no serious overfitting.

All predicted energies fall within 0.5 eV/atom of the corresponding DFT values. For wurtzite GaN structures containing defects or vacuum slabs, the deviation remains below 0.2 eV/atom, highlighting the IPA's high accuracy for capturing defects in GaN.

B. Formation energy

To validate the obtained GAP specifically for point defects in GaN, we calculated the formation energies of the defects. The formation energy $E(X)$ of a defect X at a neutral charge state was calculated as using:

$$E(X) = E_{\mathrm{tot}}(X) - \left[E_{\mathrm{tot}}(\mathrm{bulk}) + \sum_i n_i \mu_i\right] \quad (2)$$

where $E_{\mathrm{tot}}(X)$ and $E_{\mathrm{tot}}(\mathrm{bulk})$ are the total energies of a point defect X and a perfect crystal GaN, respectively. n_i is the number of atomic species i added ($n_i > 0$) or removed ($n_i < 0$) from the pristine compound. μ_i is the chemical potential of the atomic species i.

The formation energy of each defect represents its relative stability compared to a perfect crystal and determines its existence ratio in the ground state or under ideal thermal equilibrium conditions. In this study, we used 4×5×3 supercells of a primitive GaN cell, with lattice constants a, b, and c obtained by geometry optimization in DFT as $a = b = 3.222$ Å and $c = 5.824$ Å, respectively. The *k*-space mesh in the DFT calculation was set to 2×1×1. The chemical potential was set to Ga-rich condition assuming equilibrium between Ga and GaN, and between N and Mg_3N_2. The energy was calculated following geometry optimizations with fixed lattice constants.

Fig. 3 compares the formation energies of point defects in GaN under Ga-rich conditions, as calculated by DFT, our GAP model, and CHGNet without tuning [17]. The formation energies obtained by DFT were in good agreement with the reported results [18,19]. CHGNet is a pre-trained universal machine learning potential that serves as a general baseline for further training but is computationally more expensive than GAP and not tailored to specific materials.

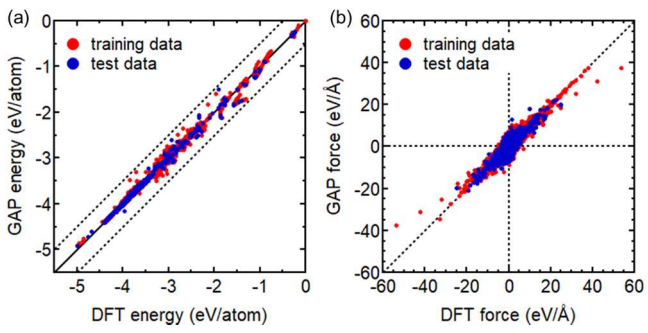

Fig. 2. (a) Cohesive energy and (b) atomic force comparison between DFT and our GAP model.

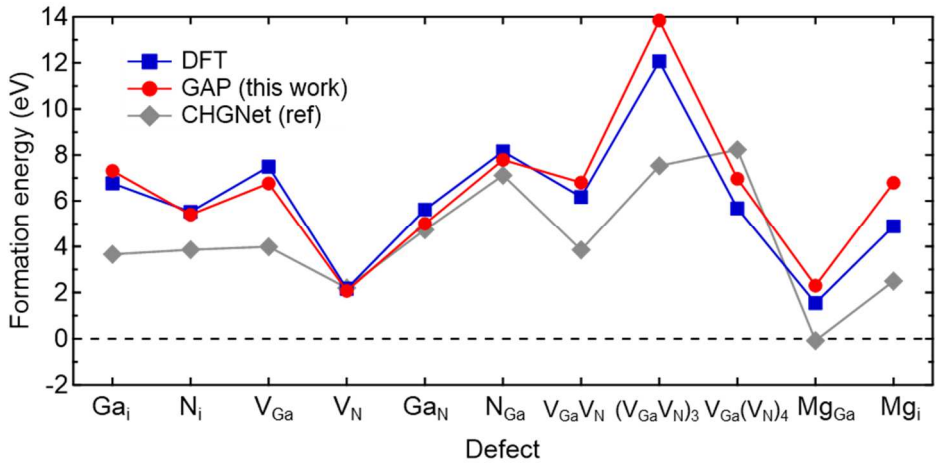

Fig. 3. Formation energies of defects in GaN calculated by DFT, our GAP model and CHGNet.

Our GAP reproduced the DFT-calculated formation energies within a maximum deviation of 1.9 eV. In contrast, the pre-trained CHGNet had a larger deviation of more than 4.5 eV. This represents a significant improvement over CHGNet, primarily because our GAP training was focused specifically on defect configurations in GaN. In particular, the accuracy of the formation energies of vacancy complexes such as $V_{Ga}V_N$ and $(V_{Ga}V_N)_3$, has improved, indicating that our GAP is well-suited for analyzing the defect recovery mechanism during post-implantation annealing, where these vacancy complexes play a crucial role [3].

C. Diffusion barrier energy

We validated our GAP in more detail using diffusion barrier energies. Diffusion barriers of defects introduced by ion implantation influence the evolution of defect configurations during the fabrication process. We used the 4×5×3 supercell of GaN, which was identical to the formation energy calculations. The *k*-space mesh was set to 1×1×1 for DFT-NEB calculations.

Fig. 4 shows the barrier energies of defect diffusion in GaN calculated by the climbing-image NEB method. The barrier energies obtained by DFT were consistent with the previous DFT results [20,21]. Our GAP model is able to reproduce the barrier energies within 0.4 eV. The pre-trained CHGNet had a larger deviation of at least 1.4 eV. Compared to CHGNet, our GAP model achieves better agreement, indicating improved accuracy not only near equilibrium but also along defect migration paths.

The diffusion barrier of a Mg interstitial along GaN[0001] direction (Mg_i-c) in Fig.4 (b) predicted by our GAP model was lower than that along GaN[1-100] direction (Mg_i-a). Fig. 4(c) shows the barrier energies of Mg_i calculated by GAP. Smooth energy profiles are obtained regardless of the diffusion direction. This anisotropic diffusion behavior is qualitatively consistent with DFT, but it is not captured by CHGNet or by an established classical potential [8]. These results underscore the effectiveness of our GAP model in capturing both static and dynamic defect properties in GaN. Because the segregation and diffusion of Mg during annealing have been reported to vary greatly depending on the implantation conditions [2,5], we expect that the accurate atomic-level analysis with our GAP will help reveal the mechanisms of Mg behavior, leading to guidelines for improving Mg ion implantation control.

IV. Conclusion

In this work, we developed a GAP interatomic potential for GaN systems containing point defects, vacancy complexes, and Mg impurities, which are critical to understanding *p*-type doping of GaN. The trained GAP accurately reproduces the DFT-calculated formation energies and diffusion barriers without signs of overfitting.

Our GAP enables large-scale MD simulations of defect dynamics in GaN, offering a valuable tool for gaining deeper insight into Mg ion implantation and guiding the optimization of *p*-type doping processes.

Acknowledgement

Financial support by the Federal Ministry of Labour and Economy, the National Foundation for Research, Technology and Development and the Christian Doppler Research Association is gratefully acknowledged.

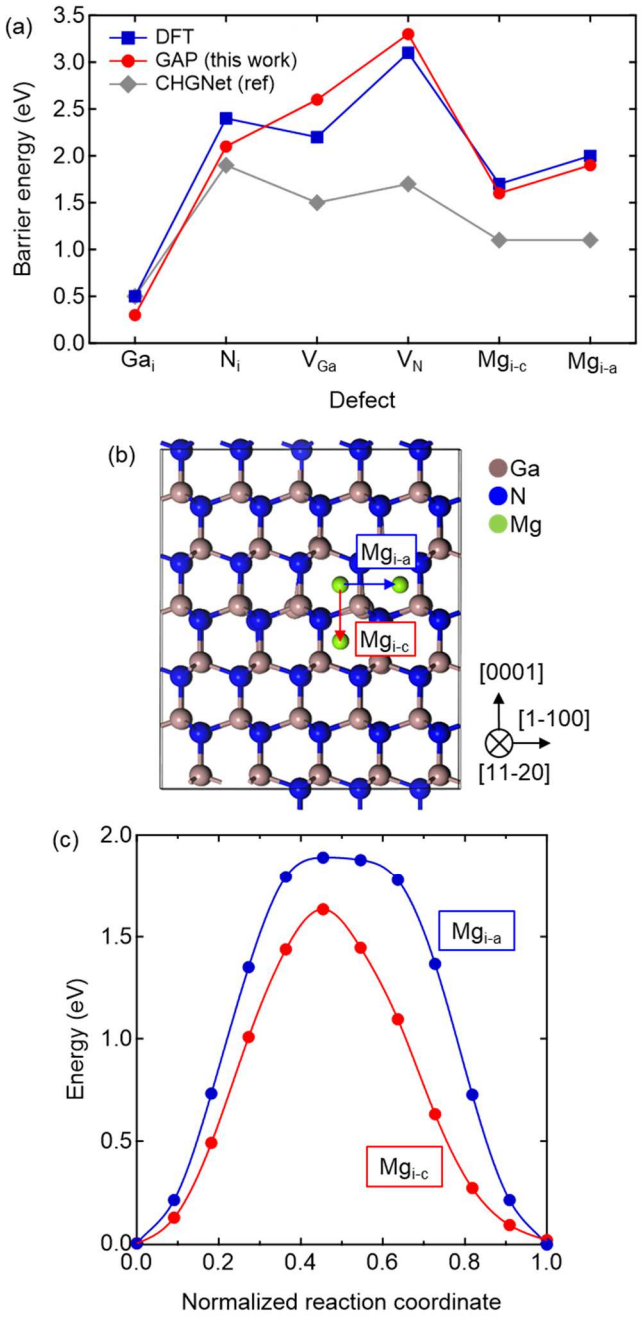

Fig. 4. (a) Barrier energies of defects in GaN calculated by DFT, our GAP model, and CHGNet. (b) Lateral view of diffusion paths for a Mg interstitial along GaN[0001] ($Mg_{i\text{-}c}$) and [1-100] ($Mg_{i\text{-}a}$) directions. (c) Energy profiles of the diffusion paths obtained by our GAP model.

REFERENCES

[1] B. J. Baliga, Semicond. Sci. Technol. **28**, 074011 (2013). doi: 10.1088/0268-1242/28/7/074011

[2] A. Uedono *et al*., Phys. Status Solidi (b) **259**, 2200183 (2022). doi: 10.1002/pssb.202200183

[3] A. Uedono *et al*., Phys. Status Solidi (b) **255**, 1700521 (2017). doi: 10.1002/pssb.201700521

[4] M. Takahashi *et al*., Jpn. J. Appl. Phys. **59**, 056502 (2020). doi : 10.35848/1347-4065/ab8b3d

[5] J. Uzuhashi *et al*., J. Appl. Phys. **136**, 055702 (2024). doi: 10.1063/5.0216601

[6] K. Iwata *et al*., J. Appl. Phys. **127**, 105106 (2020). doi: 10.1063/1.5140410

[7] K. Kataoka, T. Narita, K. Tomita, S. Yamada, and T. Kachi, Appl. Phys. Lett. **125**, 1921044 (2024). doi: 10.1002/pssb.202500029

[8] K. Harafuji, T. Tsuchiya and K. Kawamura, Jpn. J. Appl. Phys. **43**, 522 (2004). doi: 10.1143/JJAP.43.522

[9] K. Harafuji and K. Kawamura, Jpn. J. Appl. Phys. **44**, 6495 (2005). doi: 10.1143/JJAP.44.6495

[10] Z. Feng *et al*., IEEE IEDM (2024). doi: 10.1109/IEDM50854.2024.10873391.

[11] C. Song *et al*., Adv. Electron. Mater. **9**, 2300158, (2023). doi: 10.1002/aelm.202300158

[12] A. P. Bartók, M. C. Payne, R. Kondor, and G. Csányi, Phys. Rev. Lett. **104**, 136403 (2010). doi: 10.1103/PhysRevLett.104.136403

[13] V. L. Deringer *et al*., Chem. Rev. **121**, 10073 (2021). doi: 10.1021/acs.chemrev.1c00022

[14] A. P. Bartók, R. Kondor, and G. Csányi, Phys. Rev. B **87**, 184115 (2013). doi: 10.1103/PhysRevB.87.184115

[15] P. Giannozzi *et al*., J. Phys.: Condens. Matter **21**, 395502 (2009). doi: 10.1088/0953-8984/21/39/395502

[16] A. P. Thompson *et al.*, Comp. Phys. Comm. **271**, 10817 (2022). doi: 10.1016/j.cpc.2021.108171

[17] B. Deng *et al*., Nat. Mach. Intell. **5**, 1031 (2023). doi: 10.1038/s42256-023-00716-3

[18] G. Miceli and A. Pasquarello, Phys. Rev. B **93**, 165207 (2016). doi: 10.1103/PhysRevB.93.165207

[19] J. L. Lyons and C. G. Van de Walle, npj Comput. Mater. **3**, 12 (2017). doi: 10.1038/s41524-017-0014-2

[20] A. Kyrtsos, M. Maatsubara, and E. Bellotti, Phys. Rev. B **93**, 245201 (2016). doi: 10.1103/PhysRevB.93.245201

[21] G. Miceli and A. Pasquarello, Phys. Status Solidi RRL **11**, 1770337 (2017). doi: 10.1002/pssr.201700081